Chapter-3

Fabrication and Characterization of Thermally Grown $MoSe_2$ Thin Film – Based Ag/n - $MoSe_2$ / p – Si/Al Broadband Photodetector

The Part of the work is adopted from-

S. Singh and S. Jit, "**Thermally grown $MoSe_2$ thin film-based n-$MoSe_2$/p-Si broadband photodetector**," ***IEEE Transactions on Electron Devices***, vol. 71, no. 1, pp. 689–694, **Jan. 2024**, doi: 10.1109/TED.2023.3339590.

3.1 Introduction

The integration of transition metal dichalcogenides (TMDs) with silicon (Si) has become a significant area of research in broadband photodetectors due to the ability to combine the unique optical properties of TMDs with the established Si platform. Early work by Yu et al. demonstrated a MoS_2/n-Si heterojunction photodetector that exhibited broadband sensitivity from 400 to 1100 nm, leveraging the built-in electric field at the junction for self-powered operation [102]. Later studies focused on improving the performance of these heterojunctions through material optimization and interface engineering. For instance, Sarkar et al. reported a WSe_2/p-Si heterojunction photodetector that showed enhanced charge separation and responsivity [103], while Zhou et al. demonstrated a WS_2/Si heterojunction with broadband detection ranging from ultraviolet to near-infrared and improved interface quality [104]. Liu et al. extended the detection range into the near-infrared with a $MoSe_2$/Si heterojunction, achieving a high responsivity of 0.35 A/W [105]. In more recent developments, Zhang et al. designed a vertical WSe_2/Si photodetector with high responsivity and fast response time [106] and Chen et al. introduced a self-powered MoS_2/Si photodetector with enhanced stability and detectivity, demonstrating its potential for low-power applications [107]. Additionally, the incorporation of plasmonic structures, such as Au nanoparticles, has been explored to further enhance the broadband absorption in TMD/Si heterojunctions, as shown by Kumar et al. (2023)[108].

It is discussed in Chapter1 that $MoSe_2$ is a less explored material in the TMDs family for heterojunction based broadband photodetection applications possibly due to several challenges in improving the interface passivation, device scalability, and response speed of

such photodetectors. In this chapter, we have proposed an Ag/n-$MoSe_2$/p-Si/Al structure based broadband photodetector by exploring the n-$MoSe_2$/p-Si heterojunction as the photoactive region of the device. The $MoSe_2$ nanopowder synthesized by hydrothermal method has been used for $MoSe_2$ thin film deposition on the p-Si substrate by vacuum thermal evaporation method as discussed in Chapter 2. Since Al forms an Ohmic contact on p-Si whereas the Ag/n-$MoSe_2$ represents a Schottky junction as considered in Chapter 2, the proposed structure is basically a vertical series connection of the Ag/n-$MoSe_2$ Schottky junction and n-$MoSe_2$/p-Si heterojunction. The proposed photodetector shows a broadband photoresponse spectrum (300–1100 nm) covering UV-Visible-NIR wavelength region. The organization this chapter is given in the following:

Section 3.2 describes the experimental details including material synthesis and device fabrication details. The working principle using energy band diagram of the proposed structure is discussed in Section 3.3. Section 3.4 presents various results regarding the thin film characterizations and optical response characteristics of the proposed photodetector. Finally, Section 3.5 includes the summary and conclusion of this chapter.

3.2 Experimental Details

3.2.1. Materials Preparation

The material synthesis technic is similar to the method described in Chapter 2. However, it is described in brief here for the better understanding of the readers. We used all chemicals in the synthesis process bought from the Merck Chemicals and Sigma Aldrich, USA. They

were directly used without any additional processing for material synthesis and device fabrication.

For the synthesis of the active material, low-cost facile hydrothermal route was adopted. And in the process of synthesizing $MoSe_2$ nano-powder subsequent steps were followed: 1.665 g of sodium molybdate dehydrate ($Na_2MoO_4.2H_2O$), 1.58 g of selenium powder, and 0.25 g of sodium borohydride ($NaBH_4$) were dissolved in 60 mL mixed solution of absolute ethanol and de-ionized (DI) water in 1:1 volumetric ratio. After the rigorous stirring for 15 min. the resultant solution was put into a well-cleaned 100 ml Teflon-lined stainless steel autoclave. The autoclave was tightly sealed and kept in an oven subjected to the temperature of 200 ºC for 48 hrs. Thereafter, it was allowed to cool down naturally at room temperature. The black color precipitate was collected from it through centrifugation followed by several times washing through absolute ethanol and DI water subsequently. Finally, it was annealed at 60 ºC for 12 h [49], [84] to obtain $MoSe_2$ nano-powder.

3.2.2. Device Fabrication

Firstly, the Silicon wafer was diced into 15x15 mm^2 square pieces followed by subsequent cleaning in soap solution, DI water, acetone, and isopropanol in ultrasonicator bath for 10 min. each. Then the samples were dipped for 10 min. into the Pirhana solution (mixed solution of H_2O_2:H_2SO_4 in the volumetric ratio 60:40) after thorough rinsing in the running DI water (from Millipore, Milli-Q, USA) to remove residual impurities, if any. Again after thoroughly rinsing these samples in the DI water, HF solution treatment was performed for 10 min. with 10:1 volumetric ratio of DI:HF in order to remove any left-over native oxide traces. Finally, these samples were rinsed thoroughly with DI water and dried in an oven with

N_2 ambient. Then these samples were processed for plasma cleaning (Femto Science Inc., CUTE, South Korea) for 10 min in Ar:O_2 (50:50) ambient before loading the samples in the thermal evaporation unit (FL400 SMART COAT 3.0 A, Hind High Vacuum, India). The as-synthesized $MoSe_2$ powder was placed in the boat of the evaporation unit and the p-Si substrate samples were affixed by the substrate holder. Under a high vacuum condition (~2.4 × 10^{-6} mbar) inside the evaporation chamber, the thermally evaporated $MoSe_2$ material from the boat was allowed to deposit at a rate of 1.0 A/s to obtain the $MoSe_2$ thin film (~30 nm) on the p-Si substrate. For fabricating the contact electrodes on the p-Si/n-$MoSe_2$ heterostructure, Ag metal dots of 1 mm radius (with ~0.0314 cm^2 effective area) and ~100 nm thickness were deposited over the $MoSe_2$ layer followed by the deposition of a thin layer of Al (~100 nm) on the back side of the Si substrate, both at 0.2 A/s deposition rate [6], [35]. The schematic flow diagram for Device fabrication is shown in **Figure 3.1**. The schematic of the proposed device and the photograph of the fabricated device is shown in **Figure 3.2** (a) and (b) respectively.

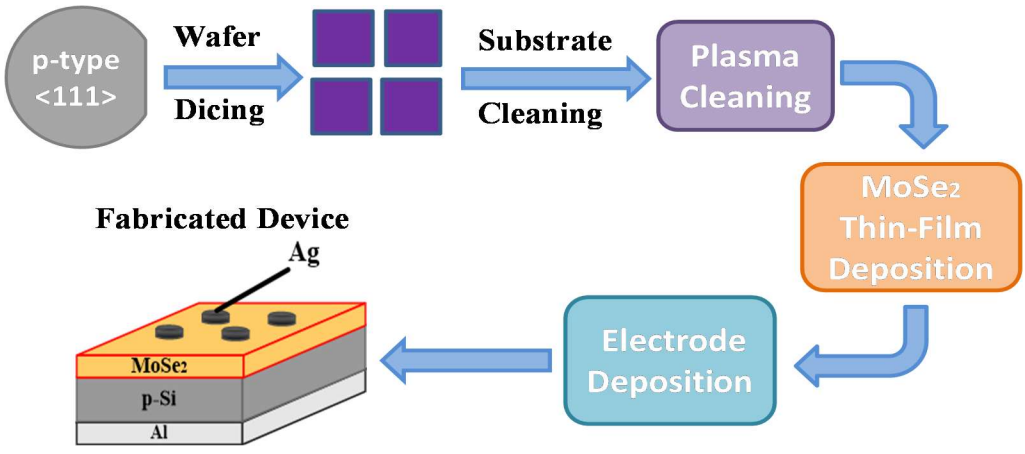

Figure 3.1 Schematic flow diagram for Device Fabrication

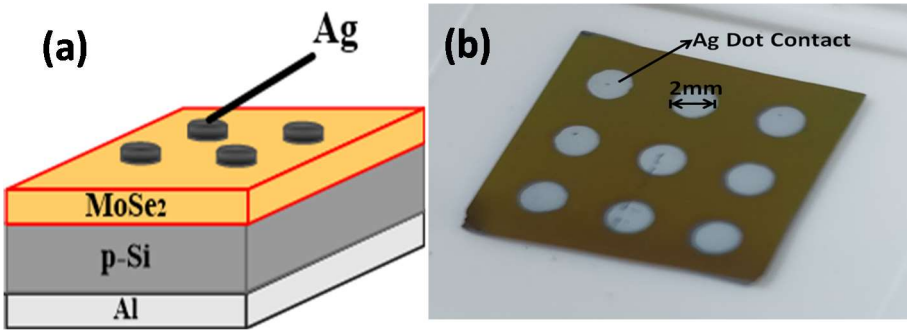

Figure 3.2 (a) Schematic device structure; (b) photograph of the fabricated device.

3.3 Energy band diagram and Working of the device

The energy band diagram of the proposed device structure is shown in **Figure 3.3** explaining the charge carrier transfer mechanism in n-$MoSe_2$/p-Si heterostructure under equilibrium, under reverse bias of 2 V in dark condition and with light illumination respectively. The conduction band, valence band, Fermi energy level, and depletion width along with their respective work function and electron affinity are shown in **Figure 3.3**. Here, we have proposed p-Si/ n-$MoSe_2$ type-II heterojunction structure. Under equilibrium as shown in **Figure 3.3** (a) fermi level on both sides are aligned after the diffusion of charge carriers across the n-$MoSe_2$/ p-Si heterojunction upon contact.

When reverse bias is applied, the shift in the alignment of the Fermi level is observed as shown in **Figure 3.3** (b). Under applied reverse bias, the depletion width broadens and increases the built-in potential which results the minority charge carrier transportation across junction producing small reverse drift current. This is also called the dark current because it is produced in reverse bias condition under dark (absence of light). Now when the light illuminates, the excess electron-hole pairs are generated mainly in the depletion region due

to absorption of light and are driven under the effect of applied reverse bias as shown in **Figure 3.3** (c). These photo-generated charge carriers under illumination are transported through the junction to produce photocurrent in the device. These photo-generated electrons in the conduction band are drifted towards the anode whereas the photo-generated holes in the valence band are drifted towards the cathode hence, producing the enhanced photon current in the device.

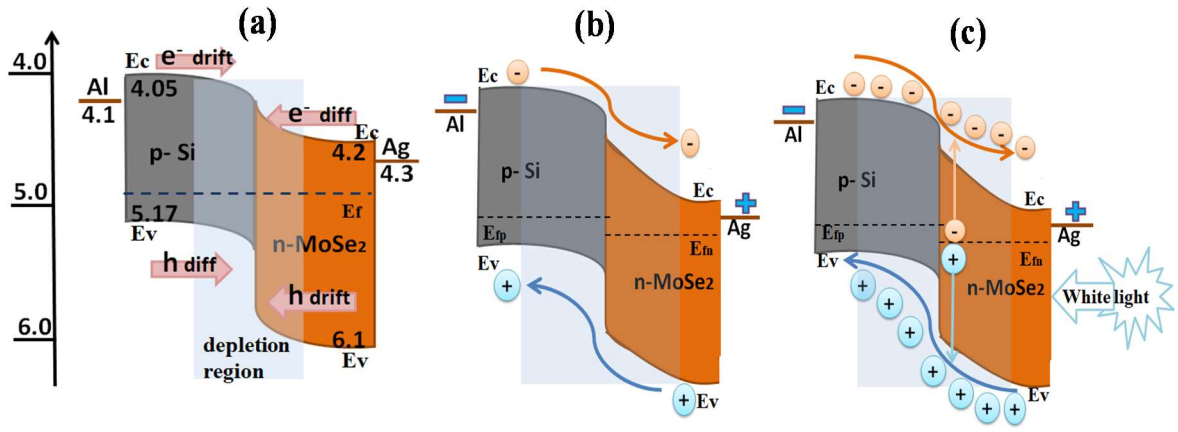

Figure 3.3 Energy band diagram (a) under equilibrium; (b) under reverse bias in dark; (c) under reverse bias with illumination.

3.4 Results and Discussion

3.4.1. Material Characterization

The crystalline phase and purity of the as-synthesized material were investigated by X-ray diffraction (XRD) using the Rigaku, SmartLab, 9 kW XRD system equipped with Cu-Kα radiation source (1.5405 Å) in continuous scan mode with XRD angle (2θ) ranging from 10º to 80º. All the peaks shown in **Figure 3.4** (a) for the XRD pattern of $MoSe_2$ are well-matched with the JCPDS card no. (29-0914). The observed diffraction peaks at 13.6º, 27.3º, 31.94º, 38.26º, 46.8º, 56.2º, 65.81º, and 70.8º correspond to (002), (004), (100), (103), (105), (110),

(200), and (203) planes, respectively, which confirm the hexagonal phase structure of the $MoSe_2$ film under study [30], [32], [33]. The as-synthesized material was also characterized by the Raman spectroscopy. **Figure 3.4** (b) shows the Raman spectroscopy of the as-synthesized $MoSe_2$ thin film using a 532 nm laser source at room temperature. Among the two distinct peaks at 240 and 288 cm^{-1} shown in the figure, the stronger peak at 240 cm^{-1} corresponds to A_{1g} mode (out-of-plane mode) and the weaker peak at 288 cm^{-1} corresponds to E^1_{2g} mode (in-plane mode) which are consistent with the previously reported works of others [48], [84].

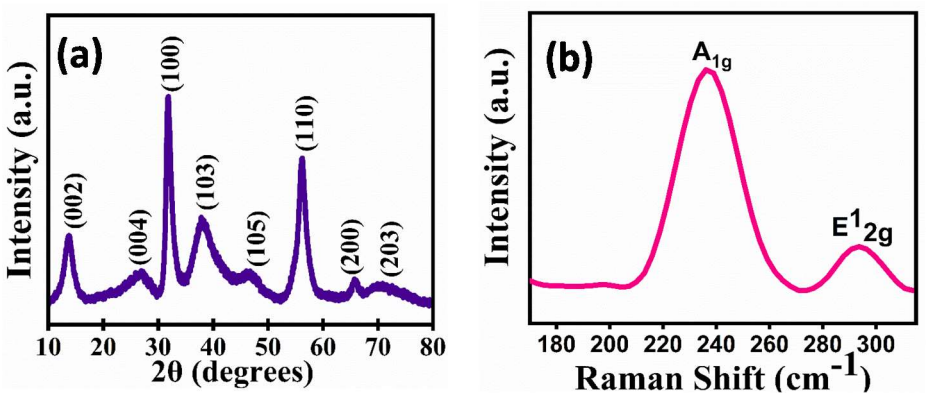

Figure 3.4 (a) XRD pattern; (b) Raman spectrum of the $MoSe_2$.

The X-ray photoelectron spectroscopy (XPS) used to investigate the chemical composition and oxidation states of the as-prepared $MoSe_2$ samples is shown in **Figure 3.5**. The spectra show the presence of Mo, Se, O, and C elements in **Figure 3.5** (a). **Figure 3.5** (b) illustrates the O 1s spectra with sharp peaks at 530 and 532 eV which are attributed to the lattice oxygen and absorbed oxygen from the environment, respectively. The high-resolution Mo 3d spectrum is shown in **Figure 3.5** (c). The peak at 228.6 eV corresponds to Mo^{4+} $3d_{5/2}$ while the peak at 231.2 eV corresponds to Mo^{4+} $3d_{3/2}$. Another small peak observed at 234.8 eV

corresponds to the Mo^{6+} oxidation state due to some residual unreacted MoO_4^{2-} introduced during the synthesis process. It may be mentioned here that the complete fabrication and characterization processes were carried out in an open environment due to the unavailability of a clean room facility. Thus, there is a chance of oxygen absorption near the surface. **Figure 3.5** (d) illustrates the high-resolution Se 3d spectra with two peaks at 54.45 and 55.28 eV corresponding to Se $3d_{5/2}$ and Se $3d_{3/2}$, respectively, which confirm the Se^{2-} oxidation state of the Se. The aforesaid data in our XPS analysis are well matched with the previously reported works of others [32], [34].

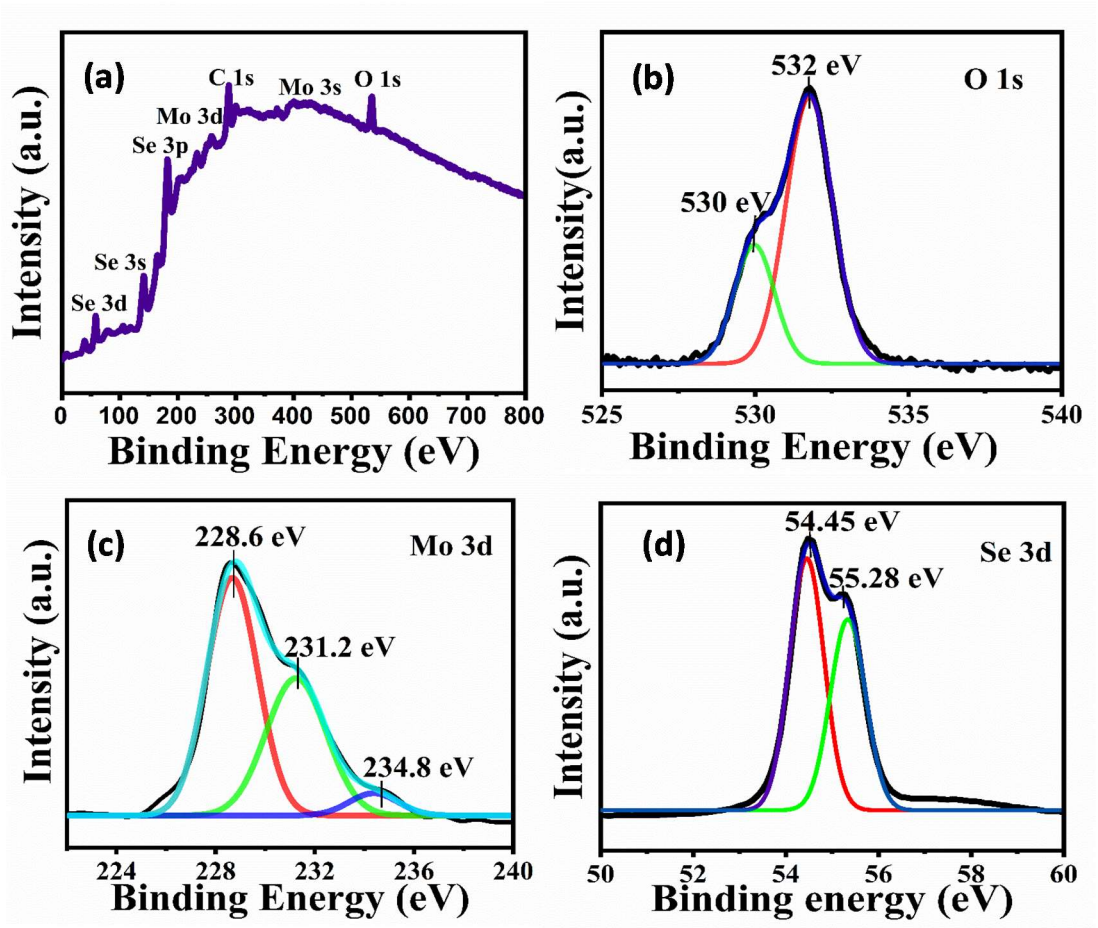

Figure 3.5 (a) XPS survey of synthesized $MoSe_2$. (b)–(d) High-resolution spectra of O 1s, Mo 3d, and Se 3d, respectively.

3.4.2. Surface and structural Characteristics

The surface morphology of the thermally grown $MoSe_2$ film was investigated through field emission-SEM (FE-SEM). **Figure 3.6** (a) shows the FE-SEM image of the thermally grown $MoSe_2$ film at 200 nm resolution. The growth of a dense uniformly distributed $MoSe_2$ film over the p-Si substrate is observed from the FE-SEM image. The surface roughness and height profile of the thermally grown $MoSe_2$ film were investigated through atomic force microscopy (AFM). The 2-D AFM image and its height profile are shown in **Figure 3.6** (b) and (c), respectively. The values of root mean square (rms) roughness and average roughness of the $MoSe_2$ film were estimated as 1.854 and 1.405 nm, respectively. The average height of the $MoSe_2$ film was estimated from the AFM height profile as ~30 nm.

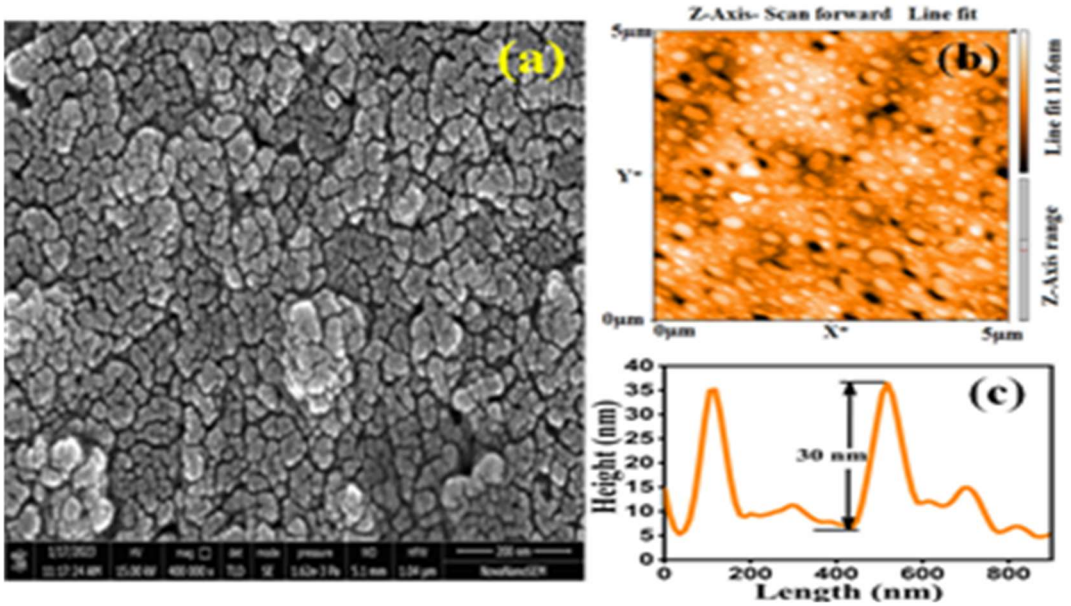

Figure 3.6 (a) FE-SEM image at 200 nm resolution; (b) 2-D AFM image; (c) AFM height profile of the $MoSe_2$ film.

3.4.3. Optical Characterization of the Device

Optical absorbance characteristics shown in **Figure 3.7** (a) of the thermally grown $MoSe_2$ thin film is measured by V-770 from JASCO, Japan. The absorbance is measured over a broad spectral range of 300–1000 nm covering the UV, Visible, and IR regions. The Tauc plot as shown in the **Figure 3.7** (b) is used to compute the optical bandgap of $MoSe_2$ thin film using the following Tauc relation [35]:

$$(\alpha h\nu)^{1/n} = \beta\,(h\nu - Eg) \qquad (3.1)$$

where β represents the band tailing parameter, and Eg is the optical band gap and n is an empirical constant. Extrapolating the leaner portion of the Tauc plot to cut the photon energy (hν) axis, Eg is estimated as ~1.9 eV.

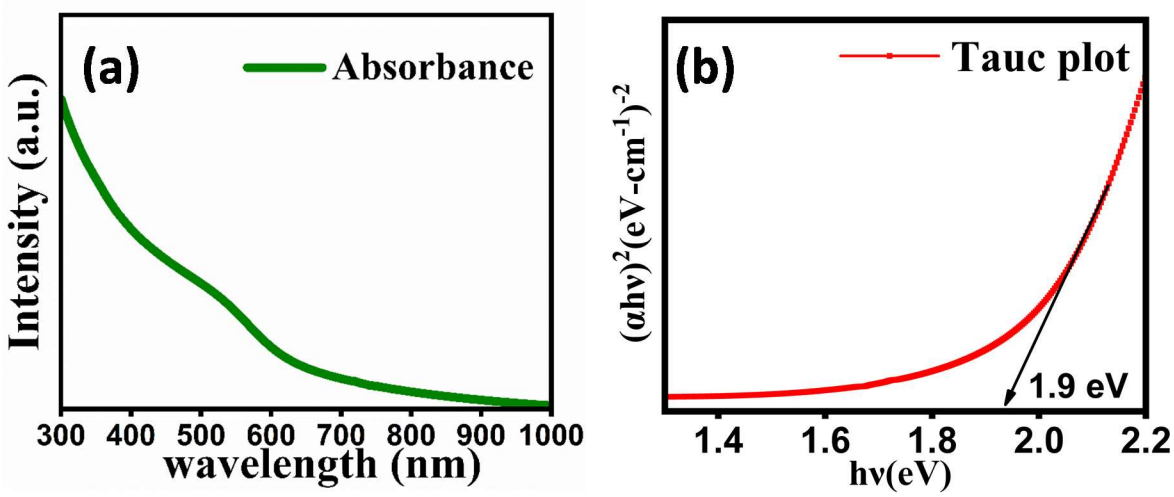

Figure 3.7 (a) Optical Absorbance; (b) Tauc plot computing bandgap of the $MoSe_2$ film.

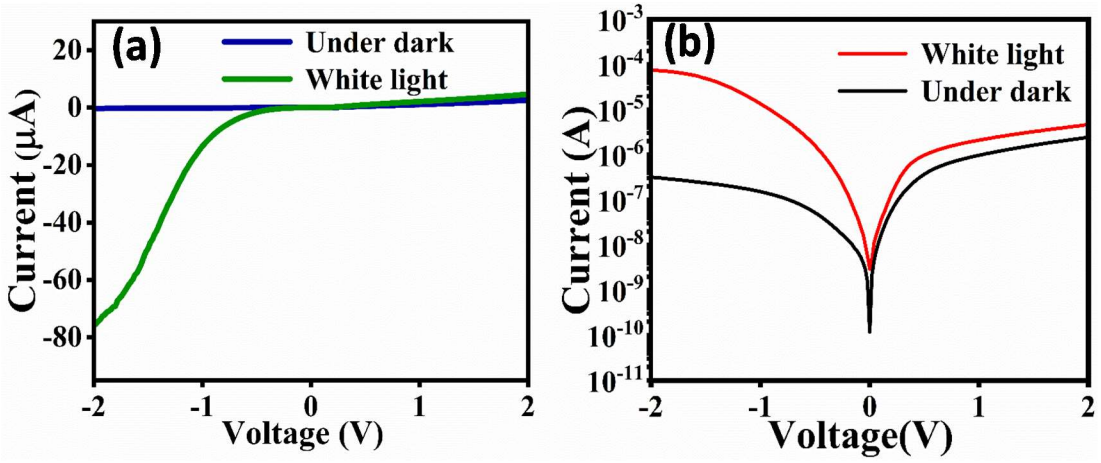

Figure 3.8 (a) I-V characteristics; (b) I-V characteristics (logarithmic scale) of the fabricated device.

3.4.4. Optoelectronics Characterization of the Device

The room-temperature current-voltage (I-V) characteristics of the fabricated p-Si/n-$MoSe_2$ heterostructure device were measured by using a semiconductor parameter analyzer (B1500A from Keysight, USA). The I-V characteristics in linear and logarithmic scale of the device measured under dark and white light illumination is shown in **Figure 3.8** (a) and (b) respectively for operating bias voltage varying from -2 V to 2 V. White light source with power density of 30 mW/cm^2 was used to illuminate the top surface of the proposed heterostructure device. The asymmetric nature of the I-V characteristics shows the rectifying nature of the device thereby confirming the formation of Si/$MoSe_2$ p-n heterojunction proposed photodetector under study.

The important performance parameters namely the responsivity and specific detectivity of the fabricated device were measured at room temperature by using monochromator (SP2150i from Princeton Instruments, USA) with a halogen light source setup. Responsivity ($R(\lambda)$), expressed in A/W, can be defined as[6], [8]:

$$R(\lambda) = \frac{Change\ in\ current/Effective\ area\ of\ the\ device}{incident\ power\ density\ on\ the\ device}$$

$$R(\lambda) = \frac{(I_{light} - I_{dark})/A_{eff}}{P_{opt}} \quad \text{A/W} \qquad (3.2)$$

where, (I_{light} - I_{dark}) is the photocurrent of the device; I_{light} and I_{dark} are the currents under illumination and dark conditions, respectively; A_{eff} is effective area of the device and P_{opt} is the incident optical power density.

The specific detectivity ($D^*(\lambda)$), an important device parameter of the photodetectors, can be expressed as [6], [8]:

$$D^*(\lambda) = \frac{R(\lambda)}{\sqrt{2eJ_d}} \quad \text{Jone} \qquad (3.3)$$

where, $R(\lambda)$: responsivity; e: charge; J_d: dark current density.

The external quantum efficiency (EQE) also an important parameter of any photodetector is expressed as[6], [8]:

$$EQE(\%) = 1240\frac{R(\lambda)}{\lambda} * 100 \qquad (3.4)$$

where, $R(\lambda)$: responsivity; λ: incident wavelength of light

Figure 3.9 shows the responsivity ($R(\lambda)$) and specific detectivity ($D^*(\lambda)$) of the fabricated device measured over 300 nm - 1100 nm spectral range. The maximum responsivity and specific detectivity were obtained as 316.25 mA/W and 1.54×10^{11} Jones at 890 nm with the applied reverse bias voltage of 2 V. **Figure 3.10** (a) shows the maximum EQE of ~45% was obtained at 890 nm under the applied reverse bias voltage of 2 V.

Finally, the response speed of the as fabricated device was investigated at room temperature by measuring the transient response characteristics of the device. A white light pulse of 10 s on-off time and power density of 30 mW/cm^2 was used to illuminate the device. The current of the photodetector was then measured as a function of time (under a reverse bias voltage of 2 V) as shown in **Figure 3.10** (b). The rise time and fall time of the output current pulse give the idea about the response speed of the device. The rise time is defined as the time taken by the current to increase from 10% to 90% of its peak value whereas the fall time is obtained as the time taken by the current to decrease from 90% to 10% of its peak value. From **Figure 3.10** (b), the rise time and fall time of the device are measured as 396 ms and 224 ms, respectively.

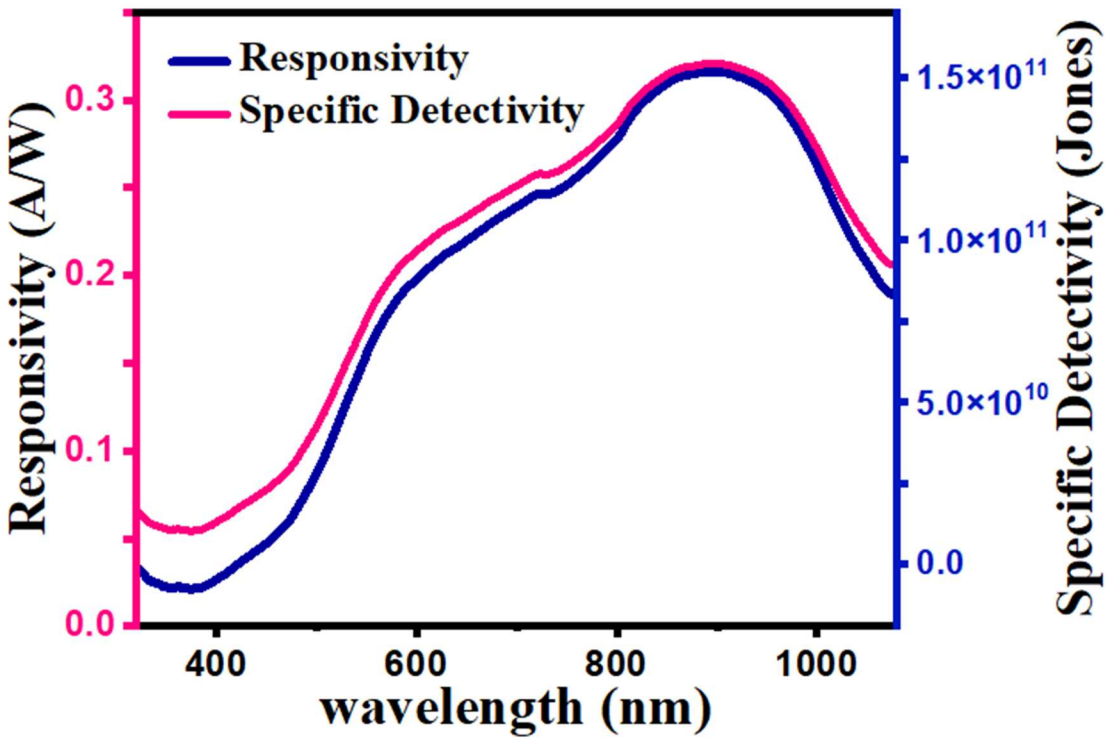

Figure 3.9 Responsivity and Specific detectivity characteristics of the fabricated device.

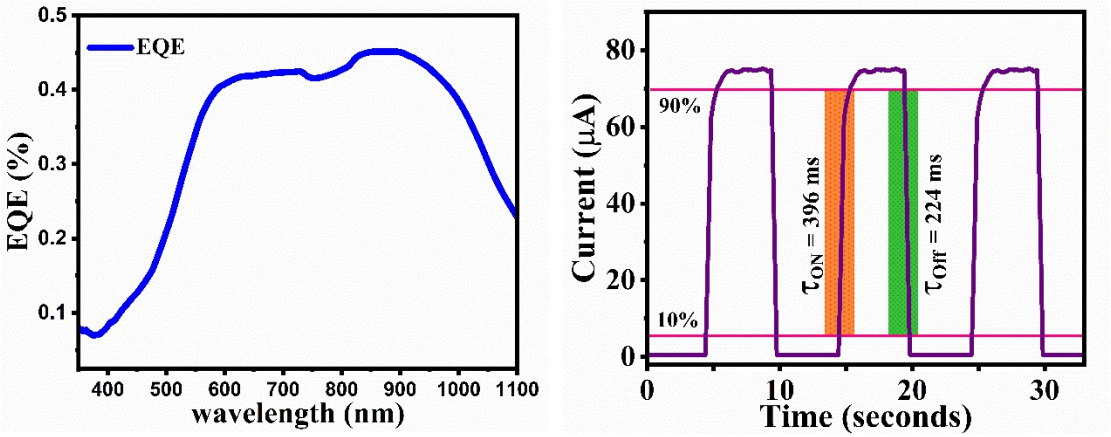

Figure 3.10 (a) EQE plot of the fabricated device; (b) Transient response characteristics of the fabricated device.

Table 3.1 Comparison of Responsivity, Detectivity, EQE and Time response of the $MoSe_2$ based photodetectors

Device Structure	**R(λ) (mA/W)**	**D(λ) (Jones)**	**EQE (%)**	**Time response**	**Ref.**
$MoSe_2$/cellulose paper	9.73	--	.015	6 s (T_{rise}) -- (T_{fall})	[56]
Gr/ $MoSe_2$/Si	270	7.13×10^{10}	-	0.27 μs (T_{rise}) 0.35 μs (T_{fall})	[64]
$MoSe_2$/ $FePS_3$	52	1.4×10^{10}	12	----------	[78]
$MoSe_2$/Gr	89.5	2.2×10^{10}	-	9.6 ms (T_{rise}) 12.8 ms (T_{fall})	[83]
$MoSe_2$ flake/SiO_2/Si	26	2.6×10^{9}	5.1	20 ms (T_{rise}) 20 ms (T_{fall})	[67]
$MoSe_2$/p-Si	**316.25**	**1.54×10^{11}**	**~45**	**396 ms (T_{rise}) 224 ms (T_{fall})**	**This work**

Various performance parameters of our proposed photodetector have been compared with some other $MoSe_2$-based heterostructure devices in **Table 3.1**. It is observed that our proposed device is better than the reported devices listed in the table.

3.5 Conclusion

The fabrication and characterization of a p-Si/n-$MoSe_2$ heterojunction based broadband photodiode have been reported in this paper. The cost-effective hydrothermal route was adopted for $MoSe_2$ synthesis. Then low-cost thermal evaporation method was used to deposit the $MoSe_2$ thin film (~30 nm) on the p-Si substrate for fabricating the proposed broadband

photodetector. The photoresponse characteristics at room temperature measured over a spectral range of 300 nm - 1100 nm exhibited the maximum responsivity of 316.25 mA/W, specific detectivity of 1.54×10^{11} Jones, and EQE of ~45% at 890 nm under a reverse bias voltage of 2 V. The rise time and fall time of the fabricated device were obtained as 396 ms and 224 ms, respectively under the reverse bias of 2 V. The performance parameters of the proposed photodetector are shown to be better than many $MoSe_2$ based heterostructure photodetectors reported in the literature.